On Computing the Underlying Fiber Directions from the Diffusion Orientation Distribution Function*

Luke Bloy[1] and Ragini Verma[2]

[1] Department of Bioengineering, University of Pennsylvania, USA
lbloy@seas.upenn.edu
[2] Department of Radiology, University of Pennsylvania, USA

Abstract. In this work, a novel method for determining the principal directions (maxima) of the diffusion orientation distribution function(ODF) is proposed. We represent the ODF as a symmetric high-order Cartesian tensor restricted to the unit sphere and show that the extrema of the ODF are solutions to a system of polynomial equations whose coefficients are polynomial functions of the tensor elements. In addition to demonstrating the ability of our methods to identify the principal directions in real data, we show that this method correctly identifies the principal directions under a range of noise levels. We also propose the use of the principal curvatures of the graph of the ODF function as a measure of the degree of diffusion anisotropy in that direction. We present simulated results illustrating the relationship between the mean principal curvature, measured at the maxima, and the fractional anisotropy of the underlying diffusion tensor.

1 Introduction

Diffusion tensor imaging (DTI) has in the past decade developed into the method of choice for investigating and characterizing white matter neural architecture non-invasively. The development of DTI has led to a number of applications in which white matter connectivity has been evaluated in both healthy and diseased populations [1,2]. Additionally, measures derived from the diffusion tensor have been widely used to characterize regional anisotropy (FA), mean diffusivity (ADC) and orientation[3]. Despite DTI's growing foothold in the imaging community, it's inability to model voxels of complex white matter, i.e. multiple fibers with different orientations, different partial volume fractions, and its dependence on a Gaussian model of diffusion within a fiber tract, has prompted the development of high angular resolution diffusion imaging (HARDI) to address these concerns.

A number of approaches have been put forth to analyze HARDI data, including the spherical harmonic decomposition of the apparent diffusion coefficient

* This work was supported by the National Institute of Health via grant R01-MH-079938.

D. Metaxas et al. (Eds.): MICCAI 2008, Part I, LNCS 5241, pp. 1–8, 2008.

(ADC) profile, the treatment of the ADC profile as a generalized tensor, q-ball imaging (QBI)[4] and persistent angular structure MRI[5]. Various scalar measures have been proposed to describe the ADC profile, including generalized anisotropy[6] and the fractional multifiber index[7]. However the maxima of the ADC profile do not necessarily coincide with the underlying fiber directions[8], making the extraction of orientation information difficult.

The correspondence between the peaks of the diffusion orientation distribution function(ODF), which describes the probability a water molecule will diffuse along a given direction, and the principal directions(PDs) of the underlying fibers, has been established experimentally[9]. For this reason a major focus within the QBI community has been directed at developing methods to compute the ODF and its maxima. A number of methods exist to compute the maxima of the ODF, such as finite difference method [10], spherical Newton's method [11] and Powell's method [5]. With the exception of the finite difference method, whose accuracy is limited to the mesh size, these methods are numerical minimization problems and thus care must be taken to avoid small local maxima, and to ensure convergence.

We present a methodology that determines the PDs of the ODF for a given voxel by computing the stationary points of the ODF. Stationary points of a function $f(u, v)$ are points where $\frac{\partial f}{\partial u} = 0$, $\frac{\partial f}{\partial v} = 0$. Each of these stationary points is then classified based on the curvature of the graph of the ODF at that point. We designate points with a curvature greater than that of a sphere with unit area, as PDs of the ODF. Figure 1, shows the graphs of representative ODFs with 1, 2 and 3 underlying fibers. Similar to the peak anisotropy described in [12], we propose the use of the mean curvature(H) at the PDs as a measure of the degree of anisotropy of the underlying fiber parallel to that direction. We present simulation results that show our method of computing the maxima is robust to noise, as well demonstrating the relationship between H and the fractional anisotropy(FA) of underlying the underlying fiber representation. Lastly we apply our method to human data to illustrate it's ability to capture the underlying directionality of fibers in fiber crossings.

2 Methods

Following the ODF calculation from the HARDI data, we expand the ODF in the real spherical harmonics, and make use of the relationship between spherical harmonics on the unit sphere and symmetric high-order Cartesian tensors to find a tensor representation of the ODF. The details of this process are discussed in section 2.1. Subsequently, we find the stationary points of the ODF, by solving a system of polynomial equations whose coefficients are given by the tensor representation of the ODF (section 2.2). The curvatures of each of these stationary points are then calculated (section 2.3) and the stationary point is classified, based on the curvature.

Notation. As the ODF is a real valued symmetric function, we use the real spherical harmonic basis of even order, as described in [13], to represent it.

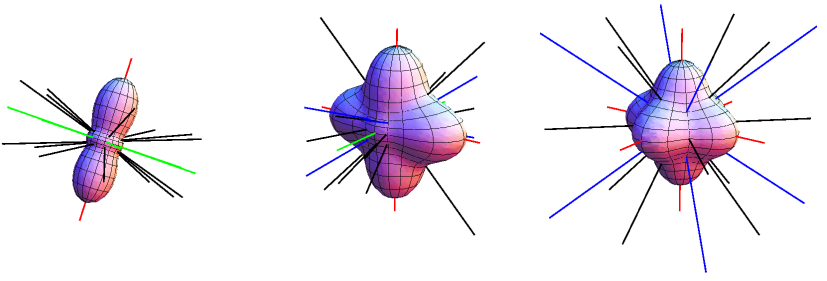

A Single Fiber **B** Two Fibers **C** Three Fibers

Fig. 1. Diffusion ODF reconstructions for simulated fiber populations. Reconstructions were performed with a tensor of rank 4. All fibers were modeled, using equation 6, with equal FA values (~ 0.85), and equal volume fractions. Red lines are the detected principal directions, green lines are secondary local maxima, blue lines are local minima and black lines are saddle points. **A**: shows a single fiber, **B**: shows two fibers oriented at right angles to one another and **C**: shows 3 fibers oriented along 3 orthogonal directions.

Namely,

$$R_j = \begin{cases} \frac{1}{\sqrt{2}}(Y_l^m + (-1)^m Y_l^{-m}) & m > 0 \\ Y_l^m & m = 0 \\ \frac{i}{\sqrt{2}}((-1)^m Y_l^m - Y_l^{-m}) & m < 0 \end{cases} \tag{1}$$

where $j = \frac{(l^2+m+2)}{2} + m$, l is even and $-l \leq m \leq l$. Also in a slight abuse of notation, we will move freely between 2 equivalent expressions for the tensor product. If f is a real homogeneous polynomial of order m, then

$$f(\boldsymbol{x}) = A\boldsymbol{x}^m = \sum_{i_1,\ldots,i_m=1}^{3} A_{i_1,\ldots,i_m} x_{i_1} \ldots x_{i_m} = \sum_{k=1}^{N} \mu_k A_k \prod_{p=1}^{m} x_{k(p)}$$

where N is the number of independent elements of A, A_k is the kth independent element of A, μ_k is the multiplicity of the element and $x_{k(p)}$ is the component of $\boldsymbol{x}$ corresponding to the pth index of the kth independent element of A.

2.1 Expressing the ODF as a Cartesian Tensor

The ODF ($\Psi(\boldsymbol{u})$) is a real valued antipodally symmetric function and thus can be expanded in the spherical harmonic basis described in equation 1. The expansion of the ODF is related to the expansion of the HARDI signal by the following relation [14,15].

$$\Psi(\boldsymbol{u}) = \sum_{j=1}^{N} 2\pi P_l(0) c_j R_j(\boldsymbol{u}) = \sum_{j=1}^{N} \psi_j R_j(\boldsymbol{u}) \tag{2}$$

where $P_l(0)$ is the Legendre polynomial of order l, $\psi_j = 2\pi P_l(0) c_j$ are the coefficients of the ODF in the R_j basis, c_j are the coefficients of the diffusion signal

in the R_j basis, and R_j are the real spherical harmonic basis functions (RSH) of equation 1.

In [13], Descoteaux et al. showed that spherical harmonics and the Cartesian tensors restricted to the unit sphere were each a basis of the same functional space and that the coefficients of the RSH expansion, $\boldsymbol{\psi} = \{\psi_k\}$ were related to the independent elements of a high-order diffusion T by $\psi = MT$ where

$$M = \begin{pmatrix} \mu_1 \int_\Omega \prod_{p=1}^{l} g_1(p) R_1(\theta,\phi) d\Omega & \dots & \mu_N \int_\Omega \prod_{p=1}^{l} g_N(p) R_1(\theta,\phi) d\Omega \\ \vdots & \ddots & \vdots \\ \mu_1 \int_\Omega \prod_{p=1}^{l} g_1(p) R_N(\theta,\phi) d\Omega & \dots & \mu_N \int_\Omega \prod_{p=1}^{l} g_N(p) R_N(\theta,\phi) d\Omega \end{pmatrix}$$

where M is a change of basis matrix and is invertible. From this and equation 2 we can represent each of the N independent elements of T as,

$$T_k = \sum_i M^{-1}_{i,k} \psi_i = 2\pi P_l(0) \sum_i M^{-1}_{i,k} c_i \tag{3}$$

Thus the $\Psi(\boldsymbol{u}) = T\boldsymbol{u}^l$, where T is a Cartesian tensor of rank l (a rank l fully-symmetric tensor has $(l^2 + 3l + 2)/2 = N$ unique components).

2.2 Finding Stationary Points

We define the tensor product Tx^{m-1} as a vector in $\mathbb{R}^3$, whose ith component is given by $\sum_{i_2,\dots,i_l=1}^{3} T_{i_1,i_2,\dots,i_l} u_{i_2} \dots u_{i_m}$. Using this definition, the method of Lagrange multipliers and the fact the T is a fully symmetric tensor, the problem of finding the stationary points of $\Psi(\boldsymbol{u}) = Tu^l$ reduces to solving the following set of homogeneous polynomial equations.

$$Tx^{l-1} = \lambda x \quad \text{s.t.} \quad x^t x = 1 \tag{4}$$

Qi [16] called a real scalar λ and a real vector u a Z-eigenvalue and a Z-eigenvector respectively if they were solutions to equation 4. Qi showed that for a given solution, x, the corresponding λ is given by $Tx^l = \Psi(x)$.

Equation 4 describes a system of homogeneous polynomial equations in 4 unknowns (x_1,x_2,x_3 and λ). We proceed by reducing equation 4 to a system of 2 variables then use the resultant of the 2 variable system to solve the system.

In practice one looks for solutions of one of three forms, $x = (1, 0, 0)$, $x = (t, 1, 0)/\left|(t, 1, 0)\right|$ and $x = (u, v, 1)/\left|(u, v, 1)\right|$, where t is the solution to an lth degree polynomial equation and where u and v are solutions to a system of 2 polynomial equations. Note that the coefficients of these polynomial equations are polynomials of the independent elements of T, and when viewed as polynomial functions of those elements, can be computed *a priori*, for a given l.

2.3 Calculating Principal Curvatures

Once the set of stationary points has been found we can calculate the corresponding curvatures, and classify each stationary point. To do this we define the surface corresponding to the graph of the ODF as

$$S = \{\Psi(\theta,\phi)(\sin(\theta)\cos(\phi), \sin(\theta)\sin(\phi), \cos(\theta)) \mid \theta \in (0,\pi), \phi \in (0,2\pi)\}$$

S is clearly a closed, orientable surface in $\mathbb{R}^3$. We choose the inward normal as our orientation, to more easily facilitate comparisons to the sphere. At a given stationary point, $p = (\theta,\phi)$, with Z-eigenvalue $\lambda = \Psi(\theta,\phi)$, we compute the Gaussian curvature (K), the mean curvature(H) and both principal curvatures (k_1,k_2) using the following equations.

$$K = \frac{eg - f^2}{EG - F^2}; H = \frac{1}{2}\frac{eG - 2fF + gE}{EG - F^2}; k_1 = H + \sqrt{H^2 - K}; k_2 = H - \sqrt{H^2 - K}$$

with $e = \lambda - \Psi_{\theta\theta}(\theta,\phi)$, $g = \lambda \sin\theta^2 - \Psi_{\phi\phi}(\theta,\phi)$, $f = -\Psi_{\theta\phi}(\theta,\phi)$ and $E = \lambda^2$, $G = \lambda^2 \sin\theta^2$, $F = 0$ and $\Psi_{\circ\circ}$ is a second order partial derivative.[17]

We can now classify p as either a principal direction (PD), secondary maxima, minima or saddle according to the following rule.

$$\text{Class of } p = \begin{cases} \text{Principal Direction} & k_1 > 4\pi, k_2 > 4\pi \\ \text{Secondary Maxima} & k_1 > k_2, 0 < k_2 < 4\pi \\ \text{Minima} & k_1 < 0, k_2 < 0 \\ \text{Saddle} & k_1 > 0, k_2 < 0 \end{cases} \tag{5}$$

Thus PDs are points where the surface, in a local neighborhood, is more convex than the sphere with unit area (the ODF of an isotropic diffusion process). If the surface is convex yet shallower than that of the sphere, we classify it as a secondary maxima. Figure 1 shows labeled ODFs for cases with 1, 2 and 3 fibers. Once the PDs have been determined we associate with each the mean curvature (H), as a measure which we relate to the FA(Figure 3).

3 Results and Discussion

Simulated Data Generation. In order to evaluate our method of calculating the principal direction, we generated HARDI signal profiles using the multi-tensor model.

$$S(\boldsymbol{u}_i) = \sum_{k=1}^{n} \frac{1}{n} e^{-b\boldsymbol{u}_i \boldsymbol{D_k} \boldsymbol{u}_i} + \text{noise} \tag{6}$$

where $i = 1, \ldots, 64$ and $\boldsymbol{u}_i$ is the gradient direction used to acquire the ith diffusion weighted signal, n is the number of fibers and $\boldsymbol{D_k}$ is the diffusion tensor of the kth fiber. In our simulations, we typically use diffusion tensors with eigenvalues $(200, 200, 1700)\text{mm}^2/\text{sec}$ at different orientations, and a b value equal to $3000 \times 10^{-6}\text{sec}/\text{mm}^2$. We computed the ODF using the RSH expansion of S according to equation 2. In both our simulations and real data results, we fit the ODF with a rank 4 diffusion tensor.

Experiments. Our first experiment was to examine the robustness of our method in the presence of noise. To this end, we generated 50 diffusion weighted

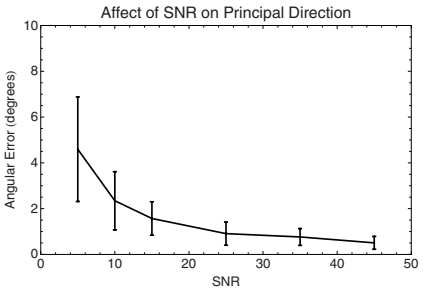

Fig. 2. Angular difference between principal direction, calculated with our method, and the principal eigenvector of the underlying tensors as a function of signal to noise ratio (SNR)

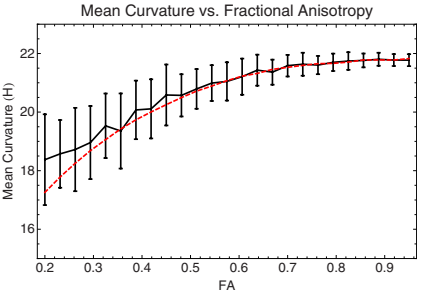

Fig. 3. Relationship between the fractional anisotropy(FA) of generating diffusion tensor and the mean principal curvature, generated without noise (dashed red line) and with SNR of 35 (solid black line)

signals, using equation 6 and a single tensor model, at six signal to noise ratios(SNRs) ranging from 5 to 45. The angle between the PD, determined using our method, and the principal eigenvector of the underlying tensor was calculated, as was the number of PDs detected. As can be seen in figure 2, even at a low SNR of 10 the mean angular error is below 5° degrees while at an SNR of 35 it drops to roughly 1° degree. As would be expected the standard deviation of the angular error decreases as the SNR increases. At a typically achievable SNR of 35 [18], our method achieves a mean accuracy of 0.7° degrees with a standard deviation of less then 0.4°. As a point of comparison a finite difference method with 1281 mesh points has a maximal accuracy of 4° degrees[10].We found that at an SNR of 10, our method correctly identified the number of PDs in 65% of the ODFs. This rate increased to 95% at SNR of 15 and 100% at SNRs $>= 20$.

Next we were interested in understanding the relationship between the FA of an underlying fiber and curvatures of the ODF at the principal direction of the fiber. We generated 50 diffusion weighted signals using a single tensor model and equation 6 with an SNR of 35, and a mean diffusivity of $700\text{mm}^2/\text{sec}$, at a number of FA values ranging from 0.2 to 0.95. For each we calculated the principal direction using our method and the mean curvature (H) of the ODF surface at that direction and compared it to the FA value. Figure 3 shows these results (solid black line), as well as the results in the absence of noise (dashed red line). These results illustrate the non-linear, monotonically increasing, relationship between FA and H. Another notable feature of figure 3 is that the standard deviation of the mean curvature decreases as the FA increases, illustrating that noise has a more pronounced effect on isotropic diffusion processes.

Finally we applied our method to diffusion weighted images acquired of healthy volunteer. Six $b = 0$ images and 64 diffusion weighted images ($b = 1000 \times 10^{-6}\text{sec/mm}^2$)were acquired. The ODF and the PDs were computed at each voxel. Figure 4 shows a representative coronal slice of RGB image, representing the principal eigenvector of the diffusion tensor, obtained through a

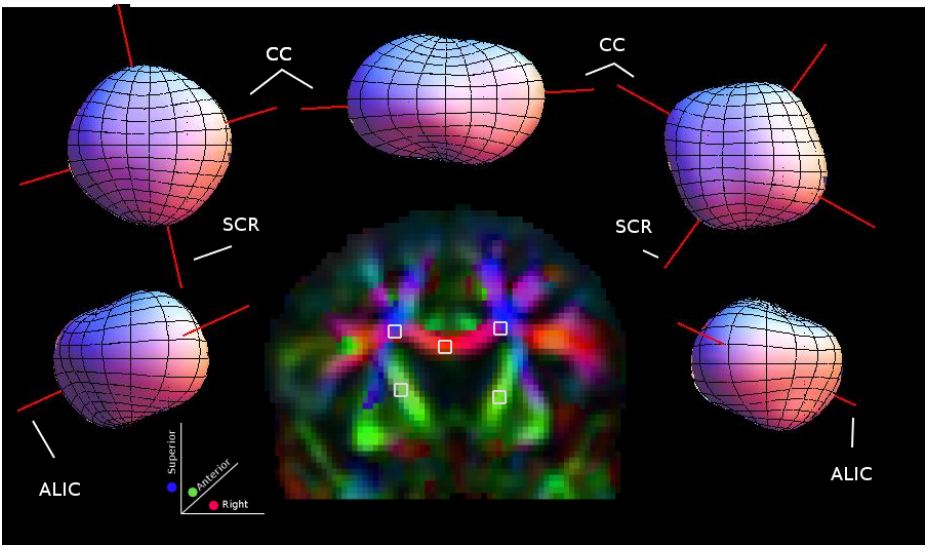

Fig. 4. Graphs showing the surface of a number of ODFs and the calculated PDs are displayed surrounding a RGB image representing the principal eigenvector of diffusion tensor. The corpus callosum (CC), the superior corona radiata (SCR) and the anterior limb of the internal capsule (ALIC) are all clearly visible as PDs of the respective graphs.

traditional DTI analysis. The surrounding graphs show the surface of the ODF along with the calculated PDs. The corpus callosum (CC), the superior corona radiata(SCR) and the anterior limb of the internal capsule (ALIC) are denoted on the graphs. Of particular importance is the ability of our method in accurately determining and distinguishing the underlying directions of the CC and the SCR in the voxels containing both.

4 Future Work

We feel that the methodology presented in this work offers a number of interesting avenues for further research. Of particularly interest is the investigation of the role that the rank of the tensor approximation has on both the accuracy of determining PDs and on the ability to distinguish two PDs that are separated by a small angle.

References

1. Wakana, S., Jiang, H., Nagae-Poetscher, L.M., van Zijl, P.C.M., Mori, S.: Fiber Tract-based Atlas of Human White Matter Anatomy. Radiology 230(1), 77–87 (2004)

2. Jellison, B.J., Field, A.S., Medow, J., Lazar, M., Salamat, M.S., Alexander, A.L.: Diffusion tensor imaging of cerebral white matter: a pictorial review of physics, fiber tract anatomy, and tumor imaging patterns. AJNR Am. J. Neuroradiol. 25(3), 356–369 (2004)
3. Basser, P.J., Pierpaoli, C.: A simplified method to measure the diffusion tensor from seven MR images. Magnetic Resonance In Medicine 39(6), 928–934 (1998)
4. Tuch, D.S.: Q-ball imaging. Magnetic Resonance in Medicine 52(6), 1358–1372 (2004)
5. Jansons, K.M., Alexander, D.C.: Persistent angular structure: new insights from diffusion magnetic resonance imaging data. Inverse Problems 19(5), 1031–1046 (2003)
6. Özarslan, E., Vemuri, B.C., Mareci, T.H.: Generalized scalar measures for diffusion MRI using trace, variance, and entropy. Magnetic Resonance in Medicine 53(4), 866–876 (2005)
7. Frank, L.R.: Characterization of anisotropy in high angular resolution diffusion-weighted MRI. Magnetic Resonance in Medicine 47(6), 1083–1099 (2002)
8. Zhan, W., Yang, Y.: How accurately can the diffusion profiles indicate multiple fiber orientations? a study on general fiber crossings in diffusion MRI. Journal of Magnetic Resonance 183(2), 193–202 (2006)
9. Perrin, M., Poupon, C., Rieul, B., Leroux, P., Constantinesco, A., Mangin, J.F., Lebihan, D.: Validation of q-ball imaging with a diffusion fibre-crossing phantom on a clinical scanner. Philos. Trans. R. Soc. Lond. B. Biol. Sci. 360(1457), 881–891 (2005)
10. Descoteaux, M.: High Angular Resolution Diffusion MRI: from Local Estimation to Segmentation and Tractography. PhD thesis, INRIA Sophia Antipolis (2008)
11. Tournier, J.D., Calamante, F., Gadian, D.G., Connelly, A.: Direct estimation of the fiber orientation density function from diffusion-weighted MRI data using spherical deconvolution. NeuroImage 23(3), 1176–1185 (2004)
12. Seunarine, K., Cook, P., Hall, M., Embleton, K., Parker, G., Alexander, D.: Exploiting peak anisotropy for tracking through complex structures. In: IEEE 11th International Conference on Computer Vision, 2007. ICCV 2007, pp. 1–8 (2007)
13. Descoteaux, M., Angelino, E., Fitzgibbons, S., Deriche, R.: Apparent diffusion coefficients from high angular resolution diffusion imaging: Estimation and applications. Magnetic Resonance in Medicine 56(2), 395–410 (2006)
14. Hess, C.P., Mukherjee, P., Han, E.T., Xu, D., Vigneron, D.B.: Q-ball reconstruction of multimodal fiber orientations using the spherical harmonic basis. Magnetic Resonance in Medicine 56(1), 104–117 (2006)
15. Descoteaux, M., Angelino, E., Fitzgibbons, S., Deriche, R.: Regularized, fast, and robust analytical q-ball imaging. Magnetic Resonance in Medicine 58(3), 497–510 (2007)
16. Qi, L.: Eigenvalues of a real supersymmetric tensor. Journal of Symbolic Computation 40(6), 1302–1324 (2005)
17. do Carmo, M.P.: Differential Geometry of Curves and Surfaces. Prentice-Hall Inc., Englewood Cliffs (1976)
18. Alexander, D.C.: Multiple-fiber reconstruction algorithms for diffusion MRI. Ann. N. Y. Acad. Sci. 1064, 113–133 (2005)